Journal of Organometallic Chemistry 884 (2019) 44–54

Contents lists available at ScienceDirect

Journal of Organometallic Chemistry

journal homepage: www.elsevier.com/locate/jorganchem

Half sandwich platinum group metal complexes of thiourea derivative ligands with benzothiazole moiety possessing anti-bacterial activity and colorimetric sensing: Synthesis and characterisation

Lathewdeipor Shadap [a], Siewdorlang Diamai [a], Venkanna Banothu [b], D.P.S. Negi [a], Uma Adepally [b], Werner Kaminsky [c], Mohan Rao Kollipara [a, *]

[a] Centre for Advanced Studies in Chemistry, North-Eastern Hill University, Shillong, 793022, India
[b] Centre for Biotechnology (CBT), Institute of Science & Technology (IST), Jawaharlal Nehru Technological University Hyderabad (JNTUH), Kukatpally, 500 085, Hyderabad, Telangana State, India
[c] Department of Chemistry, University of Washington, Seattle, WA, 98195, USA

ARTICLE INFO

Article history:
Received 23 November 2018
Received in revised form
25 January 2019
Accepted 28 January 2019
Available online 2 February 2019

Keywords:
Rhodium
Iridium
Biological and colorimetric studies

ABSTRACT

Complexes **1**–**9** were prepared by the reaction of $[(arene)MCl_2]_2$ (arene = *p*-cymene, Cp*; M = Ru, Rh and Ir) with thiourea derivative ligands **L1**, **L2** and **L3**. These complexes have been isolated as cationic bidentate (N, S), neutral bidentate (N, S) as well as neutral mono-dentate (S) complexes. Anti-bacterial activity studies were carried out for these complexes as well as the ligands against Gram-positive bacteria (*Staphylococcus aureus*) and Gram-negative bacteria (*Escherichia coli*; *Klebsiella pneumoniae*) in which all the complexes (except complexes **2** and **6**) as well as the ligands (except **L3**) showed anti-bacterial activity. In addition to the biological studies, colorimetric sensing study using silver nano-particles was also carried out where, ligands **L1** and **L3** showed agglomeration effects.

1. Introduction

Organometallic complexes have been rapidly progressing and widely explored for various medicinal and industrial purposes [1–4]. The importance of half-sandwich arene complexes have been recognized in organic synthesis due to the availability of three labile coordination sites and a rigid arene ring occupying the remaining three coordination sites [5,6]. The arene ring in these complexes plays an important role in protecting the oxidation state of the metal, influencing hydrophobicity and interaction with bio-molecules with itself being inert towards substitution [7,8].

The nature of bridging ligands mediating metal-metal interactions channels the properties of metal complexes. This role is dependent on factors such as acceptor and donor properties of coordination sites, the length and rigidity of the spacers, the availability of conjugate bonds, the orientation of substituents and scope of manipulation of ligand charge [9]. The biological behavior (anti-cancer, anti-bacterial, anti-viral, *etc.*) of metal complexes (platinum as well as non-platinum) depends on different coordination geometries, binding preferences of the coordination sites of the ligand to the metal center [10] and ligand exchange rates which are likely to lead to different mechanism(s) responsible for different biological properties. So, it is vital to take up a particular chelating ligand with known bioactive properties [11].

Literature survey related to benzothiazole compounds has revealed importance in the field of pharmaceutical applications. Compounds with benzothiazole nuclei have shown many biological activities such as antimicrobial, anti-inflammatory, anti-allergic, anti-tubercular, anti-cancer, fungicidal, anti-histamines, *etc.*, [12–20]. Varying substituents is a common method for drug design in medicinal chemistry and a useful medical value. So, from this aspect we are interested to adopt thiourea derivatives containing benzothiazole moiety as chelating ligands to the metal precursors. The thiourea ligands exhibit various binding modes [21] due to the presence of donor atoms such as N, O, and S [22] and thiourea derivatives have also shown many biological activities including anti-bacterial, anti-fungal, *etc.*, [23,24].

Previous works from this laboratory regarding thiourea-metal chemistry have shown interesting chemistry be it the modes of binding as well as anti-cancer activity of the thiourea metal complexes [25,26]. So, the importance of such work lies in the

* Corresponding author.
E-mail address: mohanrao59@gmail.com (M.R. Kollipara).

https://doi.org/10.1016/j.jorganchem.2019.01.019
0022-328X/

possibility that the next generation of thiourea derivatives incorporated with platinum d^6 metal precursors might be more efficacious as anti-bacterial agents. Apart from biological activity, the other application that the benzothiazole thiourea derivatives containing free sulfur/oxygen can have, is the sensing towards silver nanoparticles to provoke agglomeration. We aim to synthesize new thiourea derivatives and to investigate their colorimetric and biological activities.

We herein report the synthesis, characterisation and antibacterial screening of arene d^6 metal complexes containing thiourea derivatives bearing benzothiazole moiety (Chart 1).

2. Experimental

2.1. Materials and methods

The reagents were of commercial quality and used without further purification. α-phellandrene, pentamethylcyclopentadiene were purchased from Sigma Aldrich. Benzoyl isothiocyanate, 2-aminobenzothiazole, phenylisothiocyanate, benzyl isothiocyanate, silver nitrate, glutathione were obtained from Spectrochem, Alfa Aesar and S.D. fine Chem. Pvt. Ltd, Merck, HIMEDIA. The solvents were dried and distilled prior to use according to standard procedures. The ligands were prepared following the reported procedures [27–29]. Precursor metal complexes $[(arene)RuCl_2]_2$ were synthesized using reported procedure [30] and $[Cp^*MCl_2]_2$ (M = Rh/Ir) were prepared using a synthesizer, Anton par monowave 50. Using mono-wave synthesizer, in a 10 mL sample test tube, 500 mg of $Rh/IrCl_3 \cdot nH_2O$ was taken in 2 mL of methanol and 0.4 mL of Cp^* was added. The reaction was carried out for 45 min with a temperature set at 110 °C. On completion, the reaction cools down to a temperature of 60 °C. A red-orange crystalline solid was obtained. The solid was decanted, washed a few times with diethyl ether, dried and collected.

^1H NMR and ^{13}C NMR spectra were recorded on a Bruker Advance II 400 MHz spectrometer using $CDCl_3$/DMSO as solvent. Infrared spectra (KBr pellets; 400–4000 cm^{-1}) were recorded on a Perkin-Elmer 983 spectrophotometer. Mass spectra were recorded with Q-T of APCI-MS instrument (model HAB 273) using acetonitrile as solvent. Absorption spectra were recorded on a Perkin-Elmer Lambda 25 UV-Vis spectrophotometer in the range of 200–600 nm in acetonitrile at room temperature. All these complexes were synthesized and characterized by using FT-IR, ^1H NMR, ^{13}C NMR, ESI-Mass spectroscopy, UV-Vis, and single-crystal X-ray diffraction techniques.

2.2. Structure determination by X-ray crystallography

Single crystal data for the complexes were collected with Oxford Diffraction Xcalibur Eos Gemini diffractometer using graphite monochromatic Mo-Kα radiation (λ = 0.71073 Å). The strategy for the data collection was evaluated using the CrysAlisPro CCD software. Crystal data were collected by standard "phi–omega scan" techniques and were scaled and reduced using CrysAlisPro RED software. The structure solution of most of the complexes was carried out by SHELXT and refined by full-matrix least squares method based on F^2 against all reflections using SHELXL-2016 [31]. Metal atoms in the complex were located from the E-maps and all non-hydrogen atoms were refined anisotropically by full-matrix least-squares. Hydrogen atoms were placed in geometrically idealized positions and constrained to ride on their parent atoms with C–H distances in the range 0.95–1.00 A. Isotropic thermal parameters U_{eq} were fixed such that they were 1.2 U_{eq} of their parent atom Ueq for CH's and 1.5 U_{eq} of their parent atom U_{eq} in case of methyl groups. Crystallographic and structure refinement parameters for the complexes are summarized in Table 1 and selected bond lengths and bond angles are presented in Table 2. The molecular structures were drawn using ORTEP-3 [32], packing pattern and interactions like π-π, H– bonding, were drawn using MERCURY [33].

The ligands as well as the complexes have been carried out for biological activity as well as colorimetric sensing studies.

2.3. Antibacterial activity

All the Gram-negative and Gram-positive bacterial strains used for the present study were obtained from the Department of Microbiology, Osmania General Hospital, Hyderabad. All strains were tested for purity by standard microbiological methods. The bacterial stock cultures were maintained on Mueller-Hinton agar slants and stored at 4 °C. An agar-well diffusion method [34] was employed for evaluation of antibacterial activities of test compounds. DMSO was used as a negative control. The bacterial strains were reactivated from stock cultures by transferring into Mueller-Hinton broth and incubating at 37 °C for 18 h. Final inoculums containing 10^6 colonies forming units (1×10^6 CFU/mL) was added aseptically to MHA medium and poured into sterile petri dishes. Different test compounds at a concentration of 100 μg per well were added to wells (8 mm in diameter) punched on agar surface. Plates were incubated overnight at 37 °C and diameter of inhibition zone (DIZ) around each well was measured in mm. Experiments were performed in triplicates.

2.4. Colorimetric detection of ligands and complexes using silver nanoparticles

2.4.1. Synthesis of glutathione capped silver nanoparticles

100 mL of 10^{-4} M $AgNO_3$ solution was taken in a conical flask and stirred for a few minutes. To this solution 0.01 g of $NaBH_4$ was added under mild stirring. The yellow colloidal silver nanoparticles will be obtained at this step. Then 200 μL of 0.1 M NaOH was added to maintain the pH of the solution at 10. To these yellow colloidal silver NPs 100 μL of 10^{-2} M glutathione was added to stabilize the synthesized silver NPs formed. The solution was kept overnight before studies. UV-Visible spectrophotometer and Transmission Electron Microscopy (TEM) were used (Fig. 1) to characterize the synthesized silver nanoparticles.

2.5. General procedure for synthesis of metal complexes (**1**–**9**)

Metal complexes were prepared by reacting metal precursors

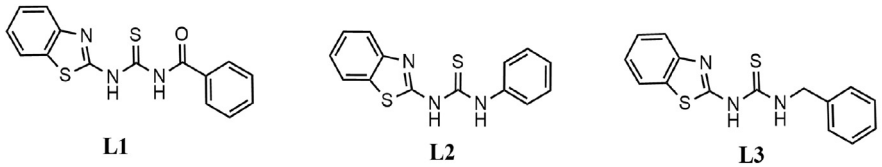

Chart. 1. Ligands used in this study.

Table 1
Crystal structure data and refinement of complexes **1, 2**, **4**, **5** and **7**.

Complexes	**[1]** Cl	**[2]**	**[4]** Cl	**[5]**	**[7]** Cl
Empirical formula	$C_{26}H_{26}Cl_4N_3ORuS_2$	$C_{25}H_{26}Cl_2N_3ORhS_2$	$C_{24}H_{25}Cl_2N_3RuS_2$	$C_{24}H_{25}ClN_3RhS_2$	$C_{25}H_{26}Cl_2N_3RuS_2$
Formula weight	703.49	622.42	591.58	557.95	604.58
Temperature (K)	293 (2)	296 (2)	298 (2)	291.72 (16)	294.5 (3)
Wavelength (Å)	0.71073	0.71073	0.71073	0.71073	0.71073
Crystal system	Monoclinic	Orthorhombic	Triclinic	Monoclinic	Monoclinic
Space group	*P 2₁/c*	*P c a 21*	*P -1*	*P 2₁/c*	*P 2₁/c*
a (Å)/α (°)	9.7636 (4)/90	17.4873 (10)/90	10.3375 (11)/73.618 (10)	13.1417 (8)/90	8.9353 (4)/90
b (Å)/β (°)	24.3519 (15)/93.932 (5)	13.9218 (10)/90	10.3732 (13)/76.909 (9)	13.6121 (6)/109.485 (6)	28.7703 (16)/101.658 (5)
c (Å)/γ (°)	12.1477 (9)/90	21.3771 (16)/90	12.3282(13)/74.933 (10)	13.7457 (7)/90	10.1148 (5)/90
Volume ($Å^3$)	2881.5 (3)	5204.4 (6)	1207.9 (3)	2318.1 (2)	2546.6 (2)
Z	4	8	2	4	4
Density (calc) (Mg/m^{-3})	1.622	1.589	1.626	1.599	1.577
Absorption coefficient	1.086	1.046	1.061	1.050	1.009
F(000)	1420	2528	600	1136	1228
Crystal size (mm^3)	0.29 × 0.25 × 0.25	0.23 × 0.16 × 0.12	0.25 × 0.23 × 0.21	0.25 × 0.23 × 0.21	0.23 × 0.21 × 0.12
Theta range for data collection	3.5990–28.391°	2–25°	3.5860–28.5480°	3.9900–28.2980°	4.0870–27.9060°
Index ranges	$-13 \le h \le 8$, $-30 \le k \le 18$, $-15 \le l \le 13$	$-11 \le h \le 23$, $-7 \le k \le 18$, $-14 \le l \le 29$	$-13 \le h \le 13$, $-13 \le k \le 13$, $-16 \le l \le 16$	$-15 \le h \le 16$, $-17 \le k \le 6$, $-17 \le l \le 16$	$-10 \le h \le 12$, $-38 \le k \le 36$, $-11 \le l < 13$
Reflections collected	11769	14532	8244	8580	10038
Independent reflections	6560 [R(int) = 0.0344]	7967 [R(int) = 0.0413]	5445 [R(int) = 0.0556]	3772 [R(int) = 0.0291]	5824 [R(int) = 0.0282]
Completeness to theta = 25.00°	99.04%	99.3%	98.89%	99.03%	99.12%
Absorption correction	Semi-empirical from equivalents	Semi-empirical from equivalents	Semi-empirical from equivalents	Semi-empirical from equivalents	Semi-empirical from equivalents
Refinement method	Full-matrix least-squares on F^2	Full-matrix least-squares on F^2	Full-matrix least-squares on F^2	Full-matrix least-squares on F^2	Full-matrix least-squares on F2
Data/restraints/parameters	6560/0/334	7967/16/631	5445/0/289	3772/0/285	5824/0/298
Goodness-of-fit on F_2	1.108	1.073	1.066	1.136	1.075
Final R indices [I > 2 sigma(I)]	R1 = 0.0666, wR2 = 0.1325	R1 = 0.0627, wR2 = 0.137	R1 = 0.0703, wR2 = 0.1696	R1 = 0.0446, wR2 = 0.0991	R1 = 0.0478, wR2 = 0.0963
R indices (all data)	R1 = 0.0919, wR2 = 0.1476	R1 = 0.0855, wR2 = 0.1524	R1 = 0.1004, wR2 = 0.1973	R1 = 0.0595, wR2 = 0.1047	R1 = 0.0614, wR2 = 0.1027
Largest diff. peak and hole ($e.Å^{-3}$)	1.396 and −0.967	2.326 and −0.938	2.510 and −1.289	1.163 and −0.458	0.647 and −0.621
CCDC No.	1880836	1880837	1880838	1880839	1880840

Structures were refined on F_0^2: w$R_2 = [\Sigma[w(F_0^2 - F_c^2)^2]/\Sigma w(F_0^2)^2]^{1/2}$, where $w^{-1} = [\Sigma(F_0^2) + (aP)^2 + bP]$ and $P = [\max(F_0^2, 0) + 2F_c^2]/3$.

Table 2
Selected bond lengths (Å) and bond angles (°) of complexes.

Complexes	1	2	4	5	7
M(1)-CNT	1.698	1.771	1.677	1.798	1.689
M(1)-N(3)	2.108 (4)	–	2.118 (5)	2.108 (4)	2.109 (3)
M(1)-S(1)	2.3569 (14)	2.370 (3)	2.3794 (16)	2.3780 (12)	2.3693 (10)
M(1)-Cl(1)	2.3990 (14)	2.364 (7)	2.4019 (18)	2.4175(13)	2.4124 (10)
M(1)-Cl(2)	–	2.500 (9)	–	–	–
N(3)-M(1)-S(1)	85.10 (12)	–	86.05 (14)	83.89 (11)	87.02 (8)
N(3)-M(1)-Cl(1)	89.65 (11)	–	87.70 (14)	92.64 (11)	85.90 (8)
S(1)-M(1)-Cl(1)	83.64 (5)	99.1 (3)	84.48 (6)	88.35 (5)	85.13 (4)
S(1)-M(1)-Cl(2)	–	84.0 (3)	–	–	–
Cl(1)-M(1)-Cl(2)	–	90.2 (3)	–	–	–

CNT represents the centroid of the arene/Cp* ring and (M = Ru, Rh and Ir).

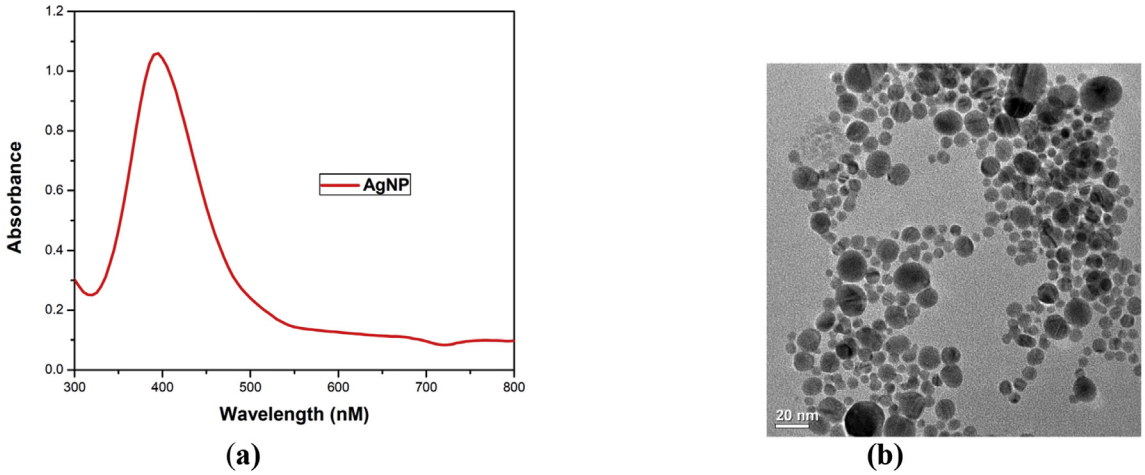

Fig. 1. (a) UV-Visible absorption spectra of Glutathione Capped silver nanoparticles (b) TEM image of Glutathione Capped silver nanoparticles.

[(arene)MCl_2]$_2$ (0.1 mmol) and thiourea derivatives (**L1, L2** and **L3**) (0.2 mmol) in dry acetone (10 mL) and stirred at room temperature for 5 h (Schemes 1–3). The solvent was concentrated under reduced pressure to 2–3 mL and on addition of 10 mL hexane, orange-yellow to pale yellow compound precipitated out. The precipitate was then washed with hexane (2 × 5 mL) and diethyl ether (2 × 10 mL) and air-dried. All these complexes are soluble in polar solvents but are insoluble in non-polar solvents.

*2.5.1. Procedure for synthesis of azido metal complex **10***

Complex **2** was treated with NaN_3 in methanol (10 mL) and stirred for 6 h at room temperature (Scheme 4). The solvent was concentrated under reduced pressure to 2–3 mL and on addition of 10 mL hexane, orange compound precipitated out. The precipitate was then washed with hexane (2 × 5 mL) and diethyl ether (2 × 10 mL) and air-dried. The complex is soluble in polar solvents but is insoluble in non-polar solvents.

*2.5.2. [(p-cymene)Ru(L1)Cl]Cl (**1**)*

Yield: (85%); yellow; FT-IR (KBr, cm^{-1}): 3434$\nu_{(NH)}$, 1633$\nu_{(C=O)}$, 1225$\nu_{(C=S)}$, 715$\nu_{(C-S)}$; ^{1}H NMR (400 MHz, $CDCl_3$) δ (ppm) = 8.49 (s, 1H, NH), 7.90 (broad s, 2H), 7.58–7052 (m, 3H), 7.45 (t, 4H, J = 8 Hz), 7.26 (t, 1H, J = 8 Hz) 5.74 (d, 1H, J = 4 Hz, $CH_{(p\text{-cym})}$), 5.46 (d, 1H, J = 8 Hz, $CH_{(p\text{-cym})}$) 5.42 (d, 1H, J = 8 Hz, $CH_{(p\text{-cym})}$) 5.36 (d, 1H, J = 4 Hz, $CH_{(p\text{-cym})}$), 2.80–2.68 (sept, 1H, $CH_{(p\text{-cym})}$), 1.90 (s, 3H), 1.19 (m, 3H), 1.1 (d, 3H, J = 4 Hz); ^{13}C NMR (100 MHz, $CDCl_3$ + DMSO): δ (ppm) = 175.75, 166.49, 151.31, 133.66, 133.56, 132.79, 128.70, 128.59, 127.50, 126.72, 125.56, 125.77, 125.14, 124.65, 124.55, 121.66, 121.60, 121.06, 120.38, 103.60, 100.34, 99.76, 88.02, 86.98, 86.05,

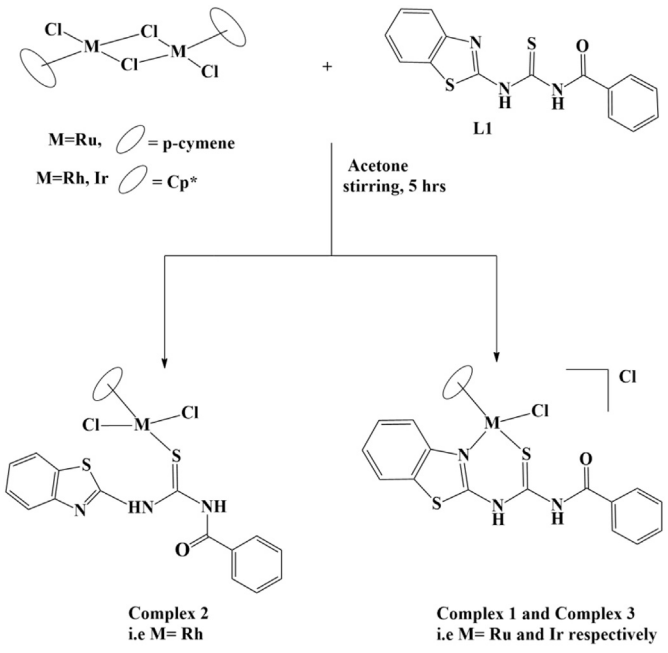

Scheme 1. Schematic representation of the synthesis of complexes **1**–**3**.

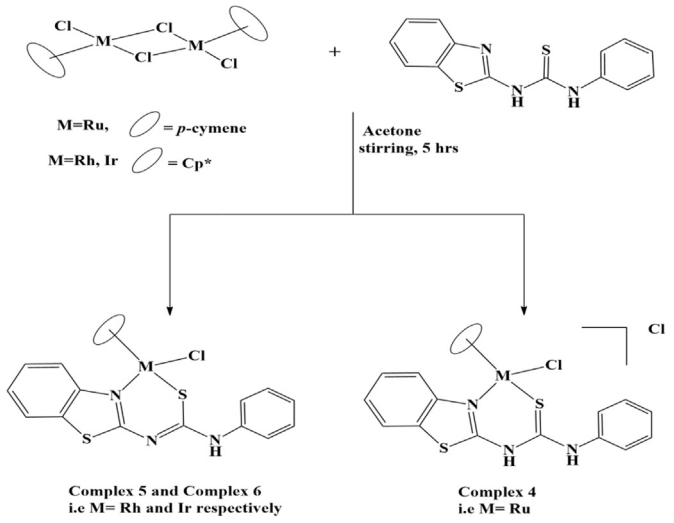

Scheme 2. Schematic representation of the synthesis of complexes **4**–**6**.

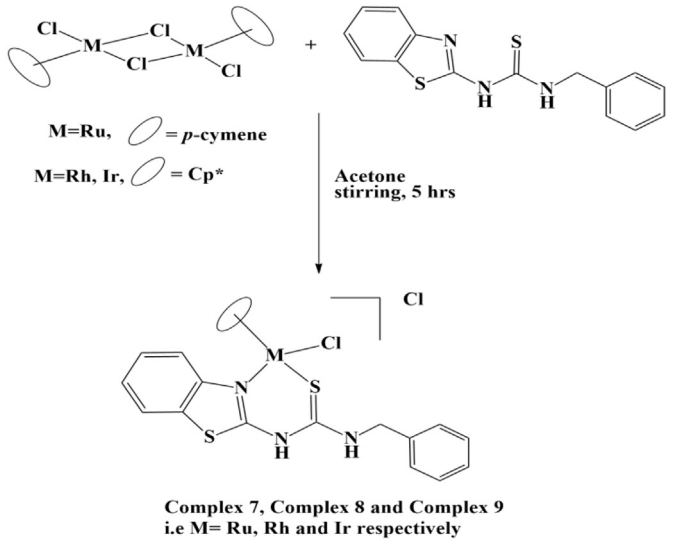

Scheme 3. Schematic representation of the synthesis of complexes **7**–**9**.

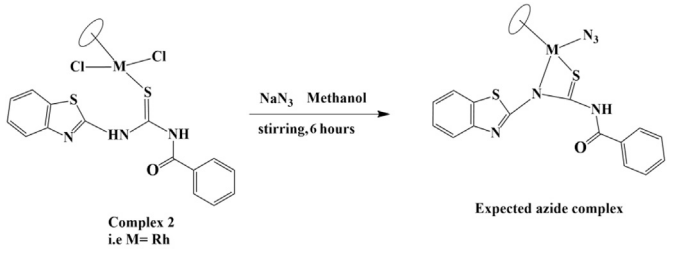

Scheme 4. Schematic representation of azido complex **10**.

85.81, 84.78, 84.68, 30.51, 23.10, 21.91, 21.57, 18.45, 18.37; MS-ESI (m/z): calculated: 548.65 $[M\text{-}2Cl]^+$, found: 547.93 $[M\text{-}2Cl]^+$; UV-Vis {Acetonitrile, λ_{max} nm ($\varepsilon/10^{-4}\,M^{-1}\,cm^{-1}$)}: 249 (1.964), 325 (1.062); Anal. Calc. for $C_{25}H_{25}Cl_2N_3ORuS_2$ (618.99) C, 48.46; H, 4.07; N, 6.78; found C, 48.53; H, 4.19; N, 6.86%.

*2.5.3. [Cp*Rh(L1)Cl$_2$] (**2**)*

Yield: (72%); orange; FT-IR (KBr, cm^{-1}): 3425$\nu_{(N-H)}$, 1638$\nu_{(C=O)}$, 1227$\nu_{(C=S)}$, 715$\nu_{(C-S)}$; ^{1}H NMR (400 MHz, $CDCl_3$): δ (ppm) = 8.52 (d, 1H, J = 8 Hz), 8.07 (broad s, 1H), 7.70 (d, 1H, J = 8 Hz), 7.62 (t, 1H, J = 8 Hz), 7.54 (t, 4H, J = 8 Hz), 7.44–7.35 (m, 2H), 1.60 (s, 15H, $CH_{(Cp^*)}$); MS-ESI (m/z): calculated: 550.54 $[M\text{-}2Cl\text{–}2H]^+$, found: 550.08 $[M\text{-}2Cl\text{–}2H]^+$; UV-Vis {Acetonitrile, λ_{max} nm ($\varepsilon/10^{-4}\,M^{-1}\,cm^{-1}$)}: 279 (2.336), 240 (2.656), 321 (10224), 369.824 (0.872); Anal. Calc. for $C_{25}H_{27}Cl_2N_3ORhS_2$ (623.44) C, 48.16; H, 4.37; N, 6.74; found C, 48.32; H, 4.52; N, 6.91%.

*2.5.4. [Cp*Ir(L1)Cl]Cl (**3**)*

Yield: (78%); light yellow; FT-IR (KBr, cm^{-1}): 3436$\nu_{(N-H)}$, 1639$\nu_{(C=O)}$, 1224$\nu_{(C=S)}$, 723$\nu_{(C-S)}$; ^{1}H NMR (400 MHz, $CDCl_3$): δ (ppm) = 8.18 (d, 1H, J = 8 Hz), 7.84 (d, 2H, J = 4 Hz), 7.53 (t, 3H, J = 8 Hz), 7.46–7.39 (m, 4H), 7.23 (d, 1H, J = 8 Hz), 1.52 (s, 15H, $CH_{(Cp^*)}$); MS-ESI (m/z): calculated: 639.85 $[M\text{-}2Cl\text{–}2H]^+$, found: 640.03 $[M\text{-}2Cl\text{–}2H]^+$; UV-Vis {Acetonitrile, λ_{max} nm ($\varepsilon/10^{-4}\,M^{-1}\,cm^{-1}$)}: 217 (3.678), 301 (1.932); Anal. Calc. for $C_{25}H_{27}Cl_2IrN_3OS_2$ (712.75) C, 42.13; H, 3.82; N, 5.75; found C, 42.22; H, 3.91; N, 5.75%.

*2.5.5. [(p-cymene)Ru(L2)Cl]Cl (**4**)*

Yield: (83%); yellow; FT-IR (KBr, cm^{-1}): 3434$\nu_{(N-H)}$, 1193$\nu_{(C=S)}$, 753$\nu_{(C-S)}$; ^{1}H NMR (400 MHz, $CDCl_3$): δ (ppm) = 11.91 (s, 1H), 8.61 (d, 1H, J = 8 Hz), 7.78 (d, 1H, J = 8 Hz), 7.67 (d, 2H, J = 8 Hz), 7.61 (t, 1H, J = 8 Hz), 7.50–7.37 (m, 5H), 5.81–5.80 (d, 1H, J = 4 Hz, $CH_{(p\text{-}cym)}$), 5.45–5.43 (d, 3H, J = 8 Hz, $CH_{(p\text{-}cym)}$), 2.85–2.76 (sept, 1H, $CH_{(p\text{-}cym)}$), 1.90 (s, 3H, $CH_{(p\text{-}cym)}$), 1.26 (d, 3H, J = 8 Hz, $CH_{(p\text{-}cym)}$), 1.17 (d, 3H, J = 8 Hz, $CH_{(p\text{-}cym)}$); MS-ESI (m/z): calculated: 519.68 $[M\text{-}2Cl\text{–}H]^+$, found: 520.00 $[M\text{-}2Cl\text{–}H]^+$; UV-Vis {Acetonitrile, λ_{max} nm ($\varepsilon/10^{-4}\,M^{-1}\,cm^{-1}$)}: 221 (4.006), 262 (1.543); Anal. Calc. for $C_{24}H_{25}Cl_2N_3RuS_2$ (591.58) C, 55.36; H, 4.84; N, 8.07; found C, 55.49; H, 4.69; N, 8.22%.

*2.5.6. [Cp*Rh(L2)Cl] (**5**)*

Yield: (71%); orange; FT-IR (KBr, cm^{-1}): 3434$\nu_{(N-H)}$, 1193$\nu_{(C=S)}$, 749$\nu_{(C-S)}$; ^{1}H NMR (400 MHz, $CDCl_3$): δ (ppm) = 8.44 (d, 1H, J = 8 Hz), 7.65–7.6 (m, 4H), 7.45 (t, 1H, J = 8 Hz), 7.38 (t, 3H, J = 8 Hz), 7.16 (s, 2H), 1.57 (s, 15H, $CH_{(Cp^*)}$); ^{13}C NMR (100 MHz, $CDCl_3$ + DMSO): δ (ppm) = 165.11, 155.02, 135.37, 127.53, 126.62, 121.36, 121.17, 120.49, 92.76, 8.63; MS-ESI (m/z): calculated: 522.53 $[M\text{-}2Cl\text{–}2H]^+$, found: 522.06 $[M\text{-}2Cl\text{–}2H]^+$; UV-Vis {Acetonitrile, λ_{max} nm ($\varepsilon/10^{-5}\,M^{-1}cm^{-1}$)}: 219 (3.162), 260 (1.520), 311 (1.092), 361 (0.935); Anal. Calc. for $C_{24}H_{27}Cl_2N_3RhS_2$ (595.43) C, 48.41; H, 4.57; N, 7.06; found C, 48.52; H, 4.69; N, 7.18%.

*2.5.7. [Cp*Ir(L2)Cl] (**6**)*

Yield: (79%); yellow; FT-IR (KBr, cm^{-1}): 3433$\nu_{(N-H)}$, 1192rd$\nu_{(C=S)}$, 749$\nu_{(C-S)}$; ^{1}H NMR (400 MHz, $CDCl_3$): δ (ppm) = 8.29 (d, 1H, J = 8 Hz), 7.65–7.59 (m, 4H), 7.52–7.33 (m, 6H), 1.56 (s, 15H, $CH_{(Cp^*)}$); ^{13}C NMR (100 MHz, $CDCl_3$ + DMSO): δ (ppm) = 167.02, 152.32, 130.93, 125.73, 121.27, 121.07, 117.90, 92.46, 8.68; MS-ESI (m/z): calculated: 611.84 $[M\text{-}2Cl\text{–}2H]^+$, found: 612.03 $[M\text{-}2Cl\text{–}2H]^+$; UV-Vis {Acetonitrile, λ_{max} nm ($\varepsilon/10^{-4}\,M^{-1}\,cm^{-1}$)}: 221 (3.465), 255 (1.601), 335 (1.680).

*2.5.8. [(p-cymene)Ru(L3)Cl]Cl (**7**)*

Yield: (78%); yellow; FT-IR (KBr, cm^{-1}): 3444$\nu_{(N-H)}$, 1117$\nu_{(C=S)}$, 754$\nu_{(C-S)}$; ^{1}H NMR (400 MHz, $CDCl_3$): δ (ppm) = 10.49 (s, 1H), 8.52 (d, 1H, J = 8 Hz), 7.67 (d, 1H, J = 8 Hz), 7.51 (t, 1H, J = 8 Hz), 7.44 (d, 3H, J = 8 Hz), 7.39–7.34 (m, 4H), 7.30 (t, 1H, J = 8 Hz) 5.65 (d, 1H, J = 4 Hz, $CH_{(p\text{-}cym)}$), 5.33 (d, 1H, J = 8 Hz $CH_{(p\text{-}cym)}$), 5.11 (broad, 2H, $CH_{(p\text{-}cym)}$), 4.95 (d, 1H, J = 12 Hz), 4.86 (d, 1H, J = 12 Hz), 2.64–2.54 (sept, 1H, $CH_{(p\text{-}cym)}$, 1.18 (s, 3H, $CH_{(p\text{-}cym)}$), 1.15 (d, 3H, J = 8 Hz, $CH_{(p\text{-}cym)}$), 1.07 (d, 3H, J = 8 Hz, $CH_{(p\text{-}cym)}$); ^{13}C NMR (100 MHz, $CDCl_3$ + DMSO): δ (ppm) = 176.56, 160.06, 149.45, 135.78, 128.83,

128.59, 128.18, 128.07, 127.40, 126.26, 124.89, 122.05, 104.08, 101.05, 88.40, 85.35, 84.89, 83.89, 83.20, 49.08, 30.49, 22.95, 21.62, 18.45; MS-ESI (*m/z*): calculated: 534.70 $[M\text{-}2Cl]^+$, found: 534.01 $[M\text{-}2Cl]^+$; UV-Vis {Acetonitrile, λ_{max} nm ($\varepsilon/10^{-4}\,M^{-1}\,cm^{-1}$)}: 226 (2.589), 302 (1.134), 355 (0.539).

2.5.9. [Cp*Rh(L3)Cl]Cl (**8**)

Yield: (77%); orange; FT-IR (KBr, cm^{-1}): 3433$\nu_{(N-H)}$, 1124$\nu_{(C=S)}$, 759$\nu_{(C-S)}$; 1H NMR (400 MHz, CDCl3): δ (ppm) = 8.45 (d, 1H, J = 8 Hz), 7.68 (d, 1H, J = 8 Hz), 7.50 (t, 1H, J = 8 Hz), 7.41–7.23 (m, 8H), 4.92–4.87 (m, 2H), 1.38 (s, 15H, $CH_{(cp^*)}$); MS-ESI (*m/z*): calculated: 536.55 $[M\text{-}2Cl\text{–}2H]^+$, found: 536.04 $[M\text{-}2Cl\text{–}2H]^+$; UV-Vis {Acetonitrile, λ_{max} nm ($\varepsilon/10^{-4}\,M^{-1}\,cm^{-1}$)}: 244 (2.488), 287 (1.931), 326 (1.049); Anal. Calc. for $C_{25}H_{29}Cl_2N_3RhS_2$ (609.46) C, 49.27; H, 4.80; N, 6.89; found C, 49.41; H, 4.69; N, 6.81%.

2.5.10. [Cp*Ir(L3)Cl]Cl (**9**)

Yield: (80%); light yellow; FT-IR (KBr, cm^{-1}): 3430$\nu_{(N-H)}$, 1129$\nu_{(C=S)}$, 749$\nu_{(C-S)}$; 1H NMR (400 MHz, CDCl3): δ (ppm) = 8.32 (d, 1H, J = 8 Hz), 7.71 (d, 1H, J = 8 Hz), 7.54 (t, 1H, J = 8 Hz), 7.46–7.31 (m, 8H), 4.94 (d, 1H, J = 4 Hz), 4.90 (d, 1H, J = 4 Hz), 1.49 (s, 15H, $CH_{(cp^*)}$); MS-ESI (*m/z*): calculated: 627.89 $[M\text{-}2Cl\text{–}2H]^+$, found: 626.07 $[M\text{-}2Cl\text{–}2H]^+$; UV-Vis {Acetonitrile, λ_{max} nm ($\varepsilon/10^{-4}\,M^{-1}\,cm^{-1}$)}: 222 (3.431), 302 (1.679).

2.5.11. [Cp*Rh(L1)N_3] (**10**)

Yield: (40%); orange; FT-IR (KBr, cm^{-1}): 3448$\nu_{(N-H)}$, 2029 $\nu_{(N3)}$,1636$\nu_{(C=O)}$, 1119$\nu_{(C=S)}$, 756$\nu_{(C-S)}$; 1H NMR (400 MHz, CDCl3): δ (ppm) = 7.94 (d, 1H, 8 Hz), 7.64 (t, 1H, J = 8 Hz), 7.52 (t, 3H, J = 8 Hz), 7.43–7.36 (m, 2H), 7.18 (t, 2H, J = 8 Hz), 1.49 (s, 15H, $CH_{(cp^*)}$); ^{13}C NMR (100 MHz, $CDCl_3$ + DMSO): δ (ppm) = 174.56, 159.81, 146.57, 134.57, 128.15, 127.86, 127.13, 126.94, 126.22, 125.28, 122.73, 121.06, 96.28, 96.26, 47.98, 8.03. Anal. Calc. for $C_{25}H_{27}N_6ORhS_2$ (594.56) C, 50.50; H, 4.58; N, 14.13; found C, 50.86; H, 4.71; N, 14.21%.

3. Results and discussion

3.1. Synthesis of metal complexes

Arene metal complexes **1**–**9** were synthesized by reacting metal precursors and the respective ligands **L1**, **L2** and **L3** in dry acetone for 5 h in the ratio of 1:2 (Schemes 1–3) while complex **10** was synthesized from complex **2** treated with NaN_3 (Scheme 4). Neutral complexes **5** and **6**, upon treatment with NaN_3 (Scheme 5) yielded no azido complexes instead oily-blackened compounds were obtained upon standing at room temperature. Complexes were isolated as cationic bidentate (N, S) mononuclear complexes, neutral bidentate (N, S) as well as neutral mono-dentate (S) complexes. Reaction of metal precursors with **L1**, yielded cationic bidentate (N, S) bonded complexes in the case of ruthenium and iridium while with rhodium, mono-dentate S bonded complex. Metal precursors with ligand **L2**, yielded cationic bidentate (N, S) bonded complex in the case of ruthenium whereas rhodium and iridium neutral bidentate complexes were formed. With ligand **L3**, all metal complexes were found to be cationic bidentate complexes. All these complexes were of good yield, air stable and soluble in solvents like dichloromethane, chloroform, methanol, acetonitrile, DMSO but insoluble in hexane, pet ether and diethyl ether.

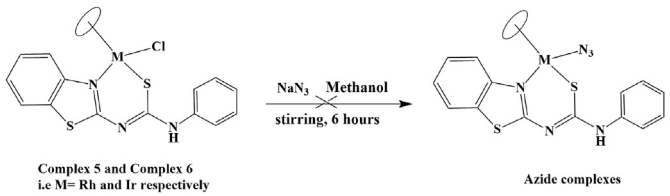

Scheme 5. Schematic representation of azido complexes.

3.2. Spectral studies of complexes

IR spectra revealed significant information between the ligands and the complexes. Stretching frequency of NH in complexes was observed in the range 3424–3444 cm^{-1} close to the range of NH stretching frequencies in free ligands (3419–3424 cm^{-1}) indicating that there was no bonding to the metal center through N–H nitrogen. In ligand **L1**, the stretching frequency of C=O was observed around 1697 cm^{-1} whereas that of complexes **1**–**3** was observed around 1703–1705 cm^{-1} signifying that there was no bonding between oxygen of carbonyl group and the metal center. The stretching frequency of C=S in free ligands was observed around the range 1188–1244 cm^{-1} whereas in the complexes, it shifted to a lower frequency *i.e.* 1117–1227 cm^{-1} indicating that no bonding through sulfur atom to the metal center [35]. This decrease in stretching frequency of C=S may be attributed to the fact that there is a delocalization of electrons from the thione sulfur to the metal on complexation which weakens the C=S. The stretching frequency of C–S in free ligands was found to be in the range 743–754 cm^{-1} where as in the complexes it was observed at around 743–769 cm^{-1}. Complex **2,** which is a neutral complex, upon treatment with NaN_3, an azido complex is formed indicated by IR peak at 2029 cm^{-1} due to N_3.

3.2.1. ^1H NMR studies of the complexes

The ^1H NMR spectra of the complexes have been provided in the supplementary information (Figs. S1-S10). Formation of the complexes was confirmed through NMR studies which showed the appearance of the ligand proton signals as well as *p*-cymene and Cp* ring protons. N–H signals were observed in the aromatic region along with aromatic protons of the ligands. It has been observed that there is an unusual splitting pattern of signal for *p*-cymene moiety in all the three complexes (**1, 4, 7**). In complex **1**, we observed the aromatic proton signals of *p*-cymene splits into four doublets in the range 5.35–5.74 ppm, while in complex **4**, two doublets around 5.81 ppm and 5.44 ppm and in complex **7**, two doublets around 5.65 ppm and 5.33 ppm and a broad singlet at 5.11 ppm. We also observed two doublets for the six-methyl protons of *p*-cymene instead of one doublet in the range 1.06–1.27 ppm. This unusual pattern can be attributed to the diastereotopic effect of the methyl protons of the isopropyl group and the methine protons of the *p*-cymene ring as well as the chirality of the metal upon coordination with thiourea ligands [36]. Septet signal for complexes **1, 4, 7** was observed around 2.80–2.68 ppm, 2.85–2.76 ppm, and 2.64–2.54 ppm respectively and singlet signal for methyl protons of *p*-cymene were observed around 1.9 ppm and 1.15 ppm respectively. In rhodium and iridium complexes, in addition to the protons of the thiourea ligands we also observed a sharp singlet around 1.38–1.6 ppm for complexes **2, 3, 5, 6, 8, 9, 10** corresponding to Cp* protons. By and large, the NMR study of all the complexes are with expected resonance and integration is consistent with the formulation of the complexes.

3.2.2. ^{13}C NMR studies of the complexes

The coordination of the ligands to the metal centers is further justified by ^{13}C NMR. The spectra of some of the complexes have been given in the supplementary data (Figs. S11-S14). The spectra displayed signals associated with the carbon of the ligands, *p*-cymene carbons and Cp* carbons. The aromatic carbon signals for

the ligands were observed around 117.90–176.56 ppm. The ring carbons of the *p*-cymene rings were observed around 83.20–101.05 ppm while that of the methyl, methine and isopropyl carbons of the *p*-cymene ring were observed around 18.37–30.51 ppm. The carbon of carbonyl group and carbon of thiol group exhibited around 175 ppm respectively. The Cp* methyl carbons were observed around 8.03–8.68 ppm and the Cp* ring carbons at 92.46–96.28 ppm. Overall, these results support the formation of the complexes.

3.2.3. Mass studies of the complexes

Mass data of all the complexes **1**–**9** have been provided in the supplementary data (Figs. S15-S23) and their values are given in the experimental section. The analyzed masses of the complexes were found to be consistent and tallied with the calculated masses. The found molecular ion peaks (for each complex) were displayed at *m*/*z*: 547.93 (**1**), *m*/*z*: 550.08 (**2**), *m*/*z*: 640.03 (**3**), *m*/*z*: 520.00 (**4**), *m*/*z*: 522.06 (**5**), *m*/*z*: 612.03 (**6**), *m*/*z*: 534.01 (**7**), *m*/*z*: 536.04 (**8**), *m*/*z*: 626.07 (**9**). The molecular ion peaks for the ruthenium complexes **1** and **7** corresponded to $[M\text{-}2Cl]^+$ while complex **4** corresponded to $[M\text{-}2Cl\text{–}H]^+$. The molecular ion peaks of the rhodium and iridium complexes corresponded to $[M\text{-}2Cl\text{–}2H]^+$. The consistent molecular ion peaks of the all complexes with the calculated mass, shows that there is a strong bonding of the arene ring (arene = *p*-cymene, Cp*) to the metal atom.

3.2.4. UV– visible description of metal complexes

The electronic spectra of the metal complexes were recorded in acetonitrile with 10^{-4} M concentrations at room temperature and spectra are provided in the supplementary data (Fig. S24). Since these complexes are d^6 low spin metal complexes, they contain filled orbitals of proper geometry at the metal centers which can interact with the low-lying π* orbitals of the ligands which may result in metal-to-ligand charge transfer (MLCT) transitions. The low energy absorption band observed in the range 301–369 nm is assigned to metal-to-ligand charge transfer (MLCT) dπ(M) to π*(L) transitions while the high energy absorption band observed in the range 217–287 nm may be attributed to ligand-centered π- π*/n-π* transfer [37].

3.2.5. Description of molecular structures of metal complexes

Getting the molecular structure of the metal complexes gives us a deeper and broader understanding about the coordination in metal complexes. Through crystallography studies we are able to determine a variety of binding modes and coordination in the metal complexes which other spectroscopic studies are unable to do so. In this structural analysis, we have been able to establish the crystal structures of some of the metal complexes. The ORTEP view of the isolated crystal structures **1, 2, 3, 4, 5** and **7** with atom numbering are presented in Figs. 2–4 and the relevant crystallographic parameters along with the details of bond lengths; bond angles are listed in Tables 1 and 2. Crystal structure of complex **3** because of large electron density around the metal center, its ORTEP view has been given just to show the structure, composition and confirmation of the metal complex. Single crystals were attached to a glass fiber and transferred to the Oxford Diffraction Xcalibur Eos Gemini diffractometer. For complexes **1**, **3**, **4** and **7**, X-ray studies showed that these complexes are cationic complexes bearing the general formula [(arene)M(L)Cl]Cl. The metal complexes featured a regular three-legged "piano stool" geometry in which the arene ring (arene = *p*-cymene, Cp*) occupied the coordination sites around the metal in $[fx]^5/[fx]^6$ manners, terminal chloride and chelating N, S donor ligand. The metal atom shows pseudo octahedral geometry with the arene ring occupying the three facial geometry acting as

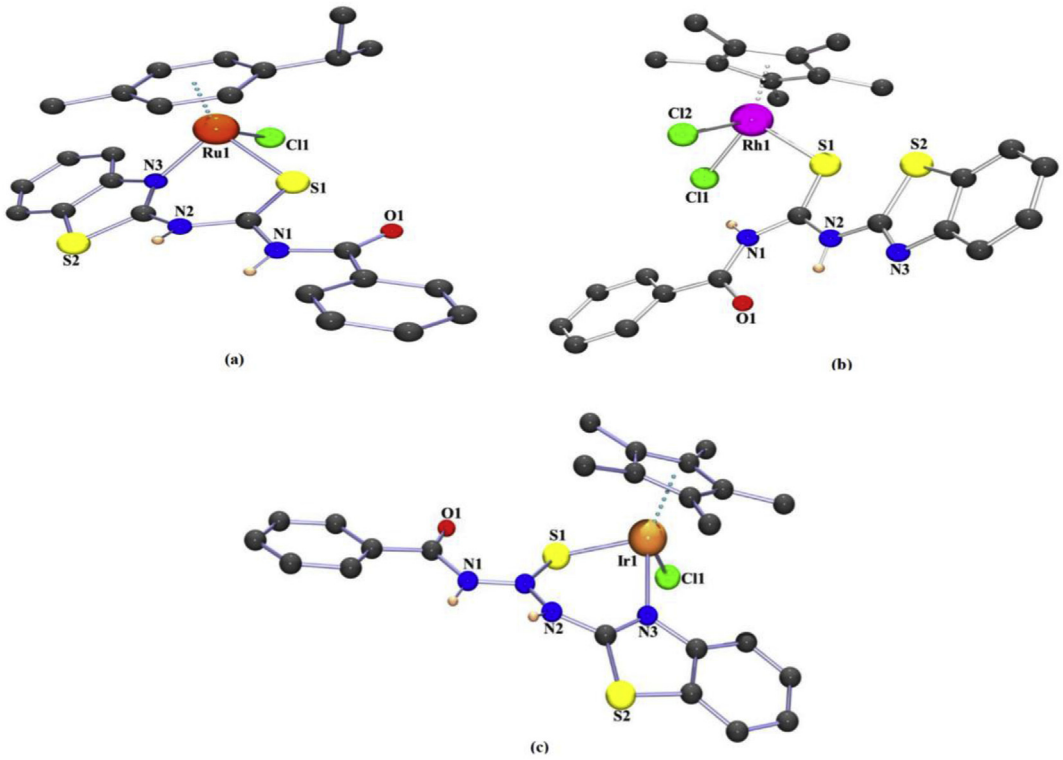

Fig. 2. (a) ORTEP diagram (ball and stick representation) of complex **1** (b) ORTEP diagram. (ball and stick representation) of complex **2** and (c) ORTEP diagram (ball and stick representation) of complex **3** is just given here to shown the composition and mode of binding of the complex. Hydrogen atoms (except NH protons) and counter ions have been omitted for clarity.

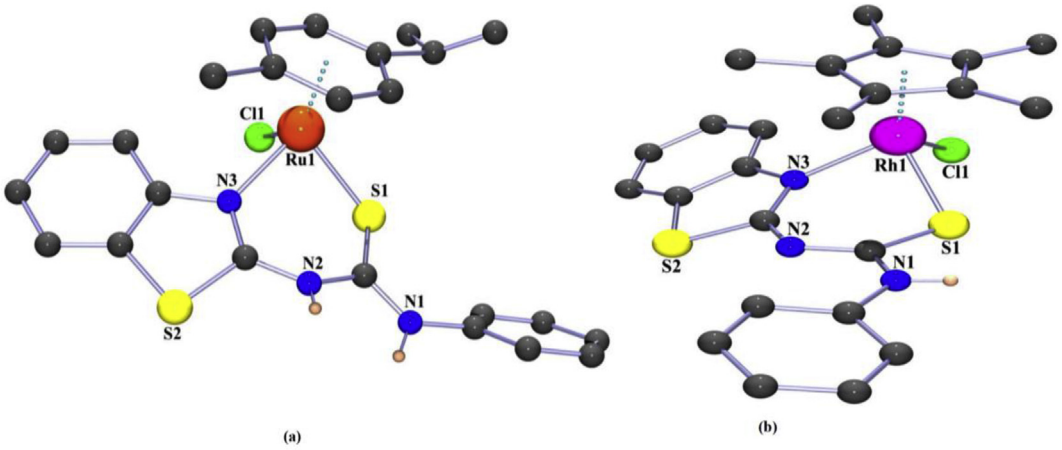

Fig. 3. (a) ORTEP diagram (ball and stick representation) of complex **4** and (b) ORTEP diagram (ball and stick representation) of complex **5**. Hydrogen atoms (except NH protons) and counter ions have been omitted for clarity.

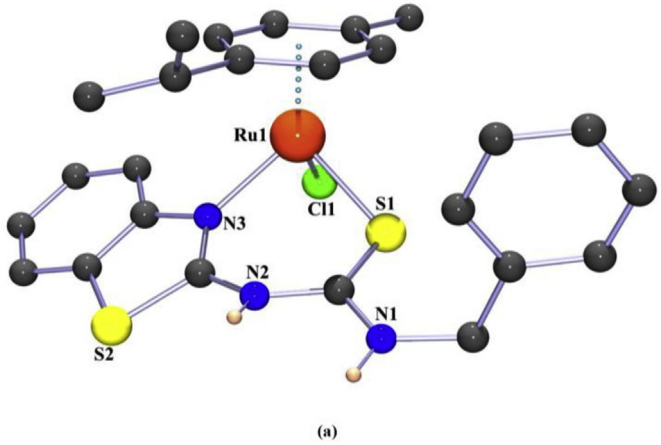

Fig. 4. ORTEP diagram (ball and stick representation) of complex **7**. Hydrogen atoms (except NH protons) and counter ions have been omitted for clarity.

the seat of a piano and the nitrogen and sulfur donor atoms from thiourea derivatives and chloride atom acting as the three legs of a piano. The molecular structures of these complexes (**1**, **3**, **4** and **7**) revealed the thiourea derivative ligands bind to the metal in a bidentate manner through nitrogen and thione sulfur donor atoms leading to the formation of a six membered chelated ring with chloride as the counter ion.

As per literature survey, thiourea derivatives are known to exhibit several binding modes. In rhodium complex **2**, we observed the binding of the ligand (**L1**) to metal center took place only through the thione sulfur, which resulted in the formation of neutral mono-dentate complex. The mode of binding occurred because there was flipping in the ligand, which made the binding through nitrogen atom of benzothiazole moiety difficult. As reported in literature [38], mono-dentate neutral complexes (S binding) when reacted with NaN_3 can result in the formation of a chelating complex with four-membered strained binding. This mode of binding in complex **2** was explored by reacting with NaN_3. Complex **2** on reacting with NaN_3 in methanol (Scheme 4) yielded azido complex **10** where the azide peak can be clearly seen through FT-IR study at around 2029 cm^{-1} while in the NMR spectrum not much of a difference was noted (Fig. S10). Unfortunately, due to the instability of crystals of the complex **10**, the molecular structure of the complex could not be obtained thereby giving us a tentative structure of a four-membered strained ring. In complex **5** and **6**, we observed that the binding of the ligand to the metal center showed a typical NS chelating binding which resulted in the formation of neutral complex where the ligand bonded to the metal through nitrogen of the benzothiazole ring and thiol sulfur (SH) upon deprotonation of thiol proton. Complex **1**, **5** and **7** crystallized in monoclinic system with space group *P* $2_1/c$, while complex **3** and **4** crystallized in triclinic system with space group *P -1* respectively while complex **2** crystallized in orthorhombic system with space group *Pca*2_1. The distance between the metal (M) to centroid of the arene/Cp* ring is 1.698(**1**) Å, 1.771(**2**) Å, 1.800(**3**) Å, 1.676(**4**) Å, 1.797(**5**) Å and 1.685(**7**) Å respectively. The metal to sulfur (M(1)-S(1)) bond distances of complexes **1**, **2**, **3**, **4**, **5** and **7** were found to be 2.3569(14) Å, 2.370(3) Å, 2.356(3) Å, 2.3794(16) Å, 2.3780(12) Å and 2.3693(10) Å respectively and the M(1)-Cl(1) bond distances of the complexes were found to be 2.3990(14) Å, 2.364(7) Å, 2.398(2) Å, 2.4019(18) Å, 2.4175(13) Å and 2.4124(10) Å respectively while in the case of complex **2** M(1)-Cl(2) was observed at 2.500(9) Å. The M – Cl bond lengths in these complexes were found to be comparable to the previous reported values [39,40]. The C–S bond distances for complexes **1**, **2**, **3**, **4** and **7** were found to be 1.669(5) Å, 1.675(10) Å, 1.681(9) Å, 1.684(6) Å and 1.683(4) Å respectively which are in good agreement with the previous reported compounds for C=S [41] whereas in complex **5**, the C–S bond distance was found to be 1.7445(5) Å which corresponded to C–S single bond. This shows that there is proton delocalization and that metal binds to sulfur as thiol sulfur.

The C=O distance for complexes **1**, **2** and **3** were found to be 1.205(7) Å, 1.218(12) Å and 1.189(12) Å respectively, which indicates to be a double bond and shows that there is no coordination to the metal centers. The bond angle values N(3)-M(1)-S(1) for complexes **1**, **3**, **4**, **5** and **7** (except complex **2** since there is no binding of metal with nitrogen of benzothiazole ring) were found to be 85.10(12)°, 85.5(2)°, 86.05(14)°, 83.89(11)° and 87.02(8)° respectively and N(3)-M(1)-Cl(1) were found to be 89.65(11)°, 89.6(2)°, 87.70(14)°, 92.64(11)° and 85.90(8)° respectively. The bond angle values S(1)-M(1)-Cl(1) for complex **1**, **2**, **3**, **4**, **5** and **7** were found to be 83.64(5)°, 99.1(3)°, 85.10(9)°, 84.48(6)°, 88.35(5)°, 85.13(4)° respectively. For complex **2**, the bond angle value S(1)-M(1)-Cl(2) and Cl(1)-M(1)-Cl(2) were

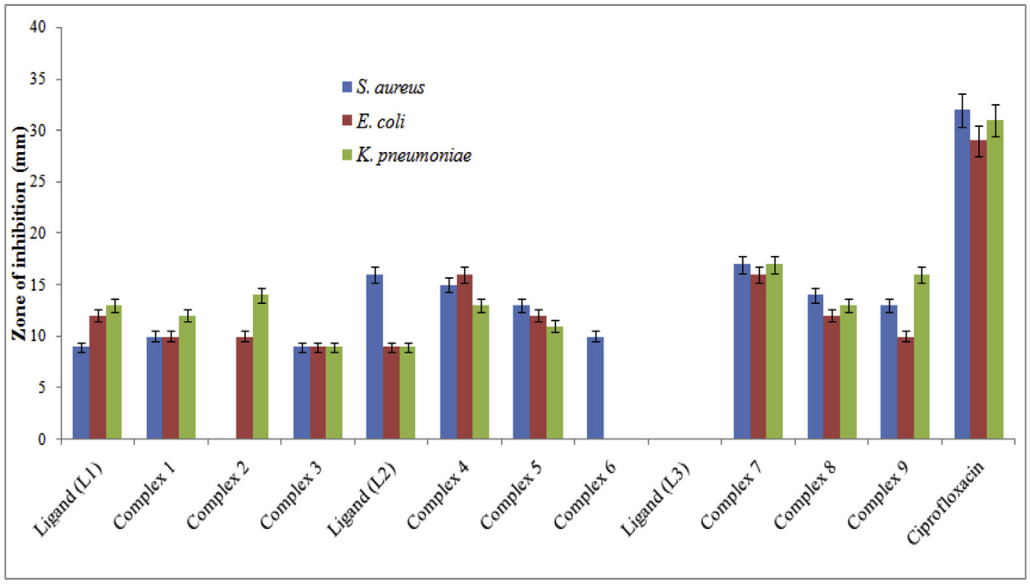

Fig. 5. Antibacterial studies of complexes **1**–**9** and ligands against Gram-positive and Gram-negative bacteria with ciprofloxacin as reference (*S. aureus* = *Staphylococcus aureus*; *E. coli* = *Escherichia coli*; *K. pneumoniae* = *Klebsiella pneumoniae*).

found to be 84.0(3)° and 90.2(3)°. The solved structure of complex **2** contains one molecule of dichloromethane.

Intramolecular, intermolecular interactions as well as π−π interactions can be seen in the crystal packing of these complexes that contributed towards the stability of the complexes (provided in the supplementary data Figs. S25–S27). Crystal packing in complex **1** (Fig. S25), showed three types of interactions *i.e* S(1)−O(1) intramolecular interaction with a distance of 2.826 Å as well as two intermolecular interactions N(1)−Cl(1) and H(4)−Cl(1) distanced at 3.291 Å and 2.876 Å respectively. In complex **2** (Fig. S25), we observed four intramolecular interactions *i.e.,* S(1)−S(2), N(1)−Cl(1) and N(1)−Cl(2) and N(2)−O(1) distanced at 3.032 Å, 3.192 Å, 3.291 Å and 2.564 Å respectively and in complex **3** (Fig. S25), we observed one intramolecular interaction S(1)−O(1) and one intermolecular interaction S(1)−H(5) distanced at 2.835 Å and 2.754 Å respectively. In complex **4** (Fig. S26), we observed inter hydrogen bonding H(1)−Cl(1) distanced at 2.913 Å and in complex **5**, (Fig. S26), two types of intermolecular interactions *i.e* S(1)−H(3) and S(1)−H(00 N) distanced at 2.623 Å and 2.908 Å respectively. In complex **7**, (Fig. S27), π-π interaction is observed distanced at 3.753 Å. These types of interactions increase the stability of the metal complexes and paves way for supramolecular motifs.

3.2.6. *In-vitro* antibacterial assay

The synthesized complexes along with the ligands were evaluated for their *in-vitro* antibacterial activity against Gram-positive Bacterium *Staphylococcus aureus* and Gram-negative bacteria *Escherichia coli*, *Klebsiella pneumoniae* by using standard techniques [42,43]. The zones of inhibition (mm) in comparison with ciprofloxacin are given in Table S1 and Fig. 5. All the compounds exhibited potent antibacterial activity against the tested organisms. *In-vitro* assay results revealed that complex **7** (17 ± 0.89 mm), ligand (**L2**) (16 ± 1.21 mm) and complex **4** (15 ± 0.57 mm) have magnificent activity against Gram-positive (*Staphylococcus aureus*). Complex **7** (16 ± 1.20 mm) and complex **4** (16 ± 0.51 mm) also showed highest activity against Gram-negative (*Escherichia coli*) while complex **7** (17 ± 1.29 mm) and complex **9** (16 ± 0.59 mm) showed more activity against Gram-negative (*Klebsiella pneumoniae*).

All the compounds except ligand (**L3**) showed significant antibacterial activity against Gram-positive and Gram-negative bacteria demonstrating their potential to be developed. However, these complexes have not superseded the antibacterial activity of the standard ciprofloxacin. Furthermore, among the complexes the ruthenium *p*-cymene complexes have shown to be effective in inhibiting the selected the bacteria.

The MIC and MBC results are listed in Table 3. The MIC and MBC values of all ligands and complexes ranged from **0.5** to **1.0** mg/mL against all the three organisms. Complex **2** values ranged from **0.25** to **0.5** mg/mL for *S. aureus* while complex **1** & **6** value ranged from **1.0** to **2.0** mg/mL. The MIC & MBC values of ciprofloxacin ranging from **0.031** to **0.062** mg/mL and **0.062** to **0.0125** mg/mL against the tested organisms was taken as standard.

3.2.7. *Colorimetric sensing studies*

Colorimetric sensing was carried out for the ligands as well as for all the complexes in room temperature. Glutathione capped silver nanoparticles was taken for the study and thiourea as the reference to the various thiourea derivatives. 20 μM of each ligand,

Table 3
Antibacterial activity (MIC & MBC) of tested compounds.

S. No.	Compound names	Stock concentration in 2.0 mg/mL					
		S. aureus		*E. coli*		*K. pneumoniae*	
		MIC	MBC	MIC	MBC	MIC	MBC
1	Ligand (L1)	0.5	1.0	0.5	1.0	0.5	1.0
2	Complex 1	1.0	2.0	0.5	1.0	0.5	1.0
3	Complex 2	0.25	0.5	0.5	1.0	0.5	1.0
4	Complex 3	0.5	1.0	0.5	1.0	0.5	1.0
5	Ligand (L2)	0.5	1.0	0.5	1.0	0.5	1.0
6	Complex 4	0.5	1.0	0.5	1.0	0.5	1.0
7	Complex 5	0.5	1.0	0.5	1.0	0.5	1.0
8	Complex 6	1.0	2.0	0.5	1.0	0.5	1.0
9	Ligand (L3)	0.5	1.0	0.5	1.0	0.5	1.0
10	Complex 7	0.5	1.0	0.5	1.0	0.5	1.0
11	Complex 8	0.5	1.0	0.5	1.0	0.5	1.0
12	Complex 9	0.5	1.0	0.5	1.0	0.5	1.0
13	Ciprofloxacin	0.062	0.125	0.031	0.062	0.062	0.125

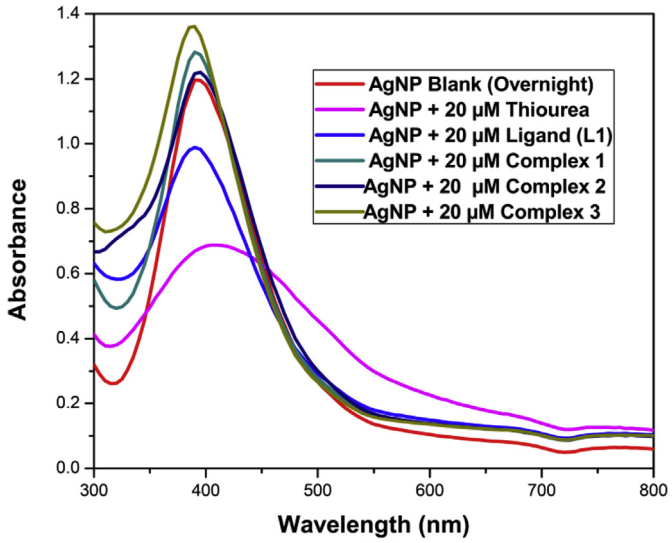

Fig. 6. SPR band of ligand **L1** and complexes **1**–**3** with thiourea as the reference.

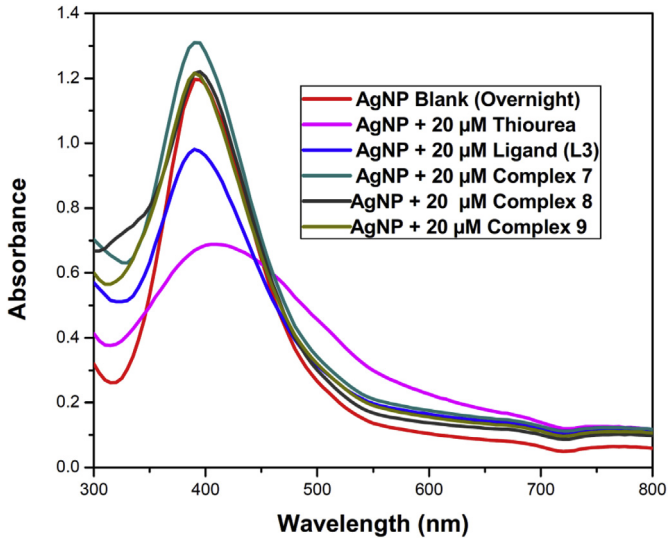

Fig. 8. SPR band of ligand **L3** and complexes **7**–**9** with thiourea as the reference.

complexes and thiourea were added to 5 mL of the silver NPs solution and kept the solutions for 2 h as well as overnight. Through UV-study, we observed that the Surface Plasmon Resonance band (SPR band) of the yellow colloidal silver nanoparticles (positioned at 395 nm) decreased upon the addition of thiourea and ligands (**L1** and **L3**) but in case of complexes the SPR band remained unchanged or slight increase in some cases. The decrease in the SPR band was due to the agglomeration of the silver NPs upon the addition of thiourea (reference) and the ligands. The agglomeration was highly effective when the solutions were kept overnight.

The decrease in the SPR band in case of the ligands is due to the fact that the ligands have free sulfur which binds on the surface of the silver NPs and causes subsequent agglomeration of the silver NPs [44], but in case of the complexes the sulfur is bonded to the metal center, hence agglomeration is hindered and no change was observed in the intensity band (Figs. 6–8). This interaction is well observed in the case of ligands (especially **L1** and **L3**).

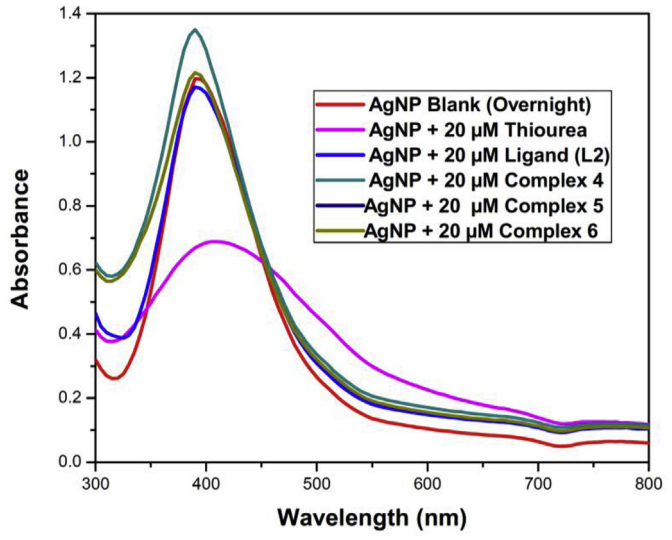

Fig. 7. SPR band of ligand **L2** and complexes **4**–**6** with thiourea as the reference.

4. Conclusion

In summary, we have successfully synthesized ruthenium, rhodium and iridium thiourea complexes. These complexes have been characterized by various spectroscopic techniques and the molecular structures of some of the complexes have been isolated. The thiourea ligands bind to the metal center in a bidentate N, S fashion forming cationic complexes with chloride as the counter ion except in complexes **5** and **6**, we observed the formation of a neutral complex while in complex **2**, the thiourea ligand (**L1**) binds to the metal center through S atom only forming a neutral monodentate complex which was further treated with NaN_3 yielding azido complex. The antibacterial activity of these complexes was evaluated against Gram-positive (*Staphylococcus aureus*) and Gram-negative (*Escherichia coli*; *Klebsiella pneumoniae*) bacteria with ciprofloxacin as the reference and colorimetric sensing was also carried out with thiourea as the reference, where all the complexes (except complexes **2** and **6**) as well as the ligands (except **L3**) showed some anti-bacterial activities while only the ligands responded to colorimetric sensing.

Acknowledgements

Lathewdeipor Shadap thanks Lincoln Dkhar for his help and contribution, CSIR, New Delhi, India for providing financial assistance in the form of CSIR NET-JRF, DST-PURSE SCXRD, NEHU-SAIF, Shillong, India for providing Single Crystal X-ray analysis and other spectral studies.

Appendix A. Supplementary data

Supplementary data to this article can be found online at https://doi.org/10.1016/j.jorganchem.2019.01.019.

References

[1] C.G. Hartinger, P.J. Dyson, Chem. Soc. Rev. 38 (2009) 391.
[2] G. Jaouen (Ed.), Bioorganometallics: Biomolecules, Labeling, Medicine, Wiley-VCH, Weinheim, Germany, 2006.
[3] C. Biot, D. Dive, Top. Organomet. Chem. 32 (2010) 155.
[4] S.Y. Mudi, T.M. Usman, S. Ibrahim, Am. J. Chem. Appl. 2 (2015) 151.
[5] L.S. Hegedus, Transition Metals in the Synthesis of Complex Organic Molecules, University Science Books, Sausalito, CA, 1999.
[6] R.D. Pike, D.A. Sweigart, Coord. Chem. Rev. 187 (1999) 183.

[7] M. Kubanik, H. Holtkamp, T. Sohnel, S.M.F. Jamieson, C.G. Hartinger, Organometallics 34 (2015) 5658.
[8] G. Gasser, I. Ott, N.M. Nolte, J. Med. Chem. 54 (2011) 3.
[9] K.T. Prasad, G. Gupta, A.K. Chandra, M.P. Pavan, M.R. Kollipara, J. Organomet. Chem. 695 (2010) 707.
[10] T. Gianferrara, I. Bratsos, E. Alessio, Dalton Trans. (2009) 7588.
[11] M. Adams, Y. Li, H. Khot, C.D. Koch, P.J. Smith, K. Land, K. Chibale, G.S. Smith, Dalton Trans. (2013) 4677.
[12] B. Rajeeva, N. Srinivasulu, S.M. Shantakumar, E- J. Inside Chem. 6 (2009) 775.
[13] I. Argyropoulou, A. Geronikaki, P. Vicini, F. Zani, ARKIVOC 6 (2009) 89.
[14] P. Venkatesh, S.N. Pandeya, Int. J. Chem. Tech. Res. 1 (2009) 1354.
[15] B.D. Naik, K.R. Desai, Asian J. Chem. 16 (2004) 1749.
[16] S.D. Srivastava, D.K. Shukla, J. Chem. Soc. 85 (2008) 306.
[17] K. Suvarna, S.P. Swain, A.M. Gandhi, Indian J. Pharmaceut. Sci. 69 (2007) 46.
[18] G.A. Kilcigil, N. Altanlar, Turk. J. Chem. 30 (2006) 223.
[19] G. Giorgioni, B. Accorroni, A.D. Stefano, G. Marucci, A. Siniscalchi, F. Claudi, J. Med. Chem. 14 (2005) 5773.
[20] M.A. Mahran, S. William, F. Ramzyv, A.M. Sembel, Molecules 12 (2007) 622.
[21] N. Selvakumaran, S.W. Ng, E.R.T. Tiekink, R. Karvembu, Ingor. Chim. Acta 376 (2011) 278.
[22] K.R. Koch, Coord. Chem. Rev. 473 (2001) 216.
[23] Y.F. Yuan, J.T. Wang, M.C. Gimeno, A. Laguna, P.G. Jones, Inorg. Chim. Acta. 324 (2001) 309.
[24] Y.M. Zhang, T.B. Wei, L. Xian, L.M. Gao, Phosphorus, Sulphur, Silicon Relat. Element. 179 (2004) 2007.
[25] S. Adhikari, O. Hussain, R.M. Phillips, W. Kaminsky, M.R. Kollipara, Appl. Organomet. Chem. 32 (2018) 4362.
[26] A. Lapsam, O. Hussain, R.M. Phillips, W. Kaminsky, M.R. Kollipara, J. Organomet. Chem. doi.org/10.1016/j.jorganchem 2018.11.020.
[27] U. Yunus, M.K. Tahir, M.H. Bhatti, S. Alib, W. Wong, Acta Crystallogr. E E64 (2008) 020.
[28] K.M. Heda, J. Appl. Chem. 4 (2015) 1541.
[29] K. Harrouche, J.F. Renard, N. Bouider, P. de Tullio, E. Goffin, P. Lebrun, G. Faury, B. Pirotte, S. Khelili, Eur. J. Med. Chem. 115 (2016) 352.
[30] (a) M.A. Bennett, T.N. Huang, T.W. Matheson, A.K. Smith, S. Ittel, W. Nickerson, Inorg. Synth. 21 (1982) 74.
[31] (a) G.M. Sheldrick, Acta Crystallogr. E ISSN 2053–2733. (b) G.M. Sheldrick, Acta Crystallogr. C 71 (2015) 3.
[32] L.J. Farrugia, J. Appl. Crystalographica. Sect. C, Struct. Chem. 71 (2015) 3.
[33] I.J. Bruno, J.C. Cole, P.R. Edgington, M. Kessler, C.F. Macrae, P. McCabe, J. Pearson, R. Taylor, Acta Crystallogr. B 58 (2002) 389.
[34] V. Banothu, A. Adepally, J. Lingam, Int. J. Pharm. Pharmaceut. Sci. 9 (2017) 192.
[35] G. Binzet, N. Kulcu, U. Florke, H. Arslan, J. Coord. Chem. 62 (2009) 3454.
[36] K.T. Prasad, B. Therrien, M.R. Kollipara, J. Organomet. Chem. 693 (2008) 3049.
[37] S. Adhikari, W. Kaminsky, M.R. Kollipara, J. Organomet. Chem. 848 (2017) 95.
[38] I.L. Mawnai, S. Adhikari, W. Kaminsky, M.R. Kollipara, J. Organomet. Chem. 869 (2018) 26.
[39] K. Jeyalakshmi, J. Haribabu, C. Balachandran, N.S.P. Bhuvanesh, N. Emi, R. Karvembu, New J. Chem. 41 (2017) 2672.
[40] M.M. Heeba, M.M. Tamizh, L.J. Farrugia, A. Endo, R. Karvembu, Organometallics 33 (2014) 540.
[41] P. Bharati, A. Bharti, M.K. Bharty, B. Maiti, R.J. Butcher, N.K. Singh, Polyhedron 63 (2013) 156.
[42] NCCLS Performance Standards for Antimicrobial Susceptibility Testing. Ninth Informational Supplement. NCCLS Document M100-S9, National Committee for Clinical Laboratory Standard, Wayne (PA), 2008.
[43] (a) V. Banothu, C. Neelagiri, A. Adepally, J. Lingam, K. Bommareddy, Pharm. Biol. 55 (2017) 1155;
(b) E.M. Lewandowski, L. Szczupak, S. Wong, J. Skiba, A. Guspiel, J. Solecka, V. Vrcek, K. Kowalski, Y. Chen, Organometallics 36 (2017) 1673.
[44] S. Diamai, W. Warjri, A. Saha, D.P.S. Negi, Colloids Surf., A 538 (2018) 593.